AIAA JOURNAL
Vol. 44, No. 6, June 2006

Structural Dynamic Considerations for a Hydrocode Analysis of Hypervelocity Test Sled Impacts

Andrew G. Szmerekovsky* and Anthony N. Palazotto†
Air Force Institute of Technology, Wright–Patterson Air Force Base, Ohio 45433

Numerical analysis of a hypervelocity test sled configuration has been accomplished with structural dynamic analysis and hydrocode analysis for investigating hypervelocity gouging. Previous studies have considered these two aspects of the system primarily apart from each other. It is desired to obtain numerical analysis of hypervelocity gouging that applies directly to a given test sled configuration. An improved analysis may be obtained for this purpose by applying structural dynamic considerations to the hydrocode analysis of slipper impacts on a rail. The primary objective of improving the input model for the hydrocode analysis is to simulate actual field conditions, such as sliding impacts with rail misalignments and on coated rails. The CTH hydrocode input model is adjusted by the addition of an artificial mass to simulate the test sled mass. Three-dimensional impacts are considered in the context of two-dimensional plane strain conditions. Shock reflections are also considered, and the results for sliding impact with a rail misalignment are discussed. The numerical results indicate characteristics seen in field gouges such as jetting and high-temperature effects.

Nomenclature

A	=	material constant
a	=	material constant in Steinberg–Guinan–Lund equation
B	=	material constant
C	=	material constant
E	=	internal energy
$f()$	=	function of
G	=	shear modulus
M	=	artificial sled system mass
m	=	thermal material constant in Johnson–Cook[11] constitutive equation
N	=	material constant
P	=	pressure
S	=	magnitude of deviatoric stress tensor
T	=	temperature
u_x	=	horizontal impact velocity, x-direction velocity of slipper
u_y	=	vertical impact velocity, y-direction velocity of slipper
Y	=	yield stress
β	=	fitting parameter in Steinberg–Guinan–Lund equation
Γ	=	Grüneisen function used in Mie–Grüneisen equation of state
γ	=	Grüneisen coefficient used in Steinberg–Guinan–Lund constitutive model
ε	=	effective strain
ε_i	=	fitting parameter in Steinberg–Guinan–Lund equation
η	=	density ratio
θ_h	=	homologous temperature
κ	=	preexponential factor
ρ	=	density
σ	=	effective stress
$2U_K$	=	energy necessary to form pair of kinks in dislocation segment

Subscripts

A	=	at Hugoniot elastic limit
M, m	=	melting
mo	=	melting at constant volume in Steinberg–Guinan–Lund model
o	=	original
P	=	Peierl's stress
R	=	value on reference curve such as Hugoniot, isentrope, or zero-Kelvin isotherm
r	=	reference
T	=	thermally activated component of yield stress in Steinberg–Guinan–Lund model
ρ	=	at constant density

Superscripts

n	=	work hardening coefficient
p	=	plastic
$\cdot$	=	rate with respect to time

I. Introduction

GOUGING (the removal of material by interacting contact surfaces) continues to be a concern for hypervelocity rail test sleds. The effects of gouging vary from requiring repair to the rail to catastrophic failure. If one observes Fig. 1, which shows the important divisions of the Holloman High Speed Test Track (HHSTT) rocket sled, it can be stated that the rocket is held to the rail using slippers (also called shoes). These slippers are made of VascoMax 300, a high-strength maraging steel. The slippers are not tight, leaving a small gap on one side or another. This results in the sled riding in free flight with intermittent contact on the steel rail (1080 steel) at velocities of Mach 10 in air. The impact between the slipper and rail may result in gouging. The main divisions of the rocket sled that are discussed in this paper are the sled system, that is, the rocket, payload, and other structures; the rails; and the slippers.

Gouges are characterized by the shallow removal of material from the rail and the slipper and have been observed to occur at sled speeds greater than 1.5 km/s (Ref. 1). Additionally, the problem is quite complex, in which materials may change phase, stress waves become important, and heat generation must be traced. The current means of mitigating gouges is to coat the rail with a polymer, such as epoxy. This has reduced the occurrence of gouging, but it is not possible to obtain a uniform coating thickness with current application methods. As velocities increase, it is not understood whether coating variations will act to increase gouging or continue to mitigate the phenomenon during test sled runs. In addition, the effect

Received 4 October 2004; revision received 18 July 2005; accepted for publication 26 July 2005.

*Assistant Professor, Department of Engineering Mechanics; aszmere@adelphia.net.

†Professor, Department of Aerospace Engineering. Associate Fellow AIAA.

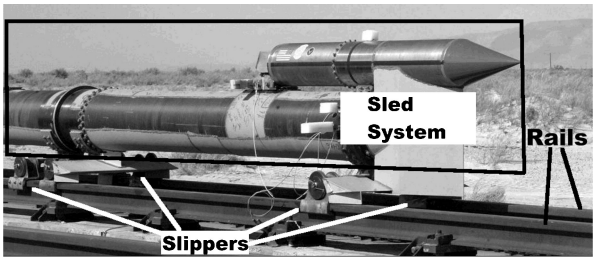

Fig. 1 HHSTT rocket sled with sled system payload, slippers, and rails labeled.

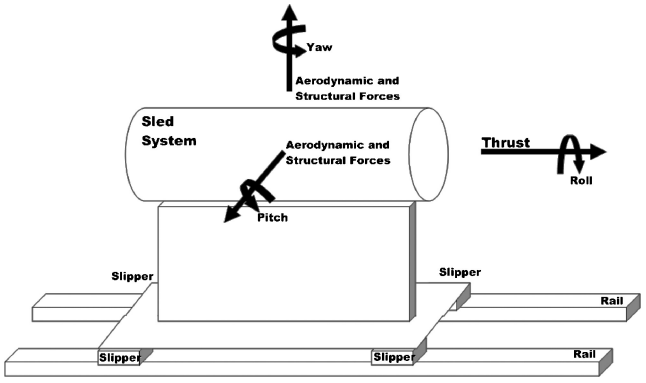

Fig. 2 Test sled schematic with motion axes.

of nonequilibrium thermodynamics on the thermal environment before impact of the slipper/shoe with the rail/guider has not been investigated fully. These scenarios must be studied, but it would do no good if the model did not depict real dimensionality.

Gouging has been studied using test track runs and observations[2] and experimentally using rail guns.[3] These findings indicate that gouging occurs under conditions of high-speed sliding, high temperature, large strain rate, plasticity, and high stress. They also suggest that there is a mixing of slipper and rail materials during gouging. Gouging has also been studied numerically using the finite volume hydrocode CTH.[4] Direct application of these numerical results to actual hypervelocity gouging requires subjective engineering judgment. For instance, slipper models with vertical impact velocities designed to match the kinetic energy of test sled vertical impacts have been used[5,6] as one means of approximating a real impact. However, this approach does not approximate the momentum of the impact unless the test sled mass is also simulated. As a consequence, results based on this model can be applied only from a phenomenological perspective. This study seeks to make conclusions that will relate directly to applications at the HHSTT at Holloman Air Force Base, New Mexico. Previous work has shown that a two-dimensional plane strain model is a reasonable model for gouging.[7]

Test data indicate that gouging occurs primarily at the corners of the rail and at other points in which a plane strain condition would occur in the three-dimensional model.[1,3] Examples of regions with plane strain conditions are impacts on a rail misalignment, a reentrant corner of the rail, or a collision of the shoe due to roll, pitch, or yaw.

The rocket sled is simplified as shown in Fig. 2. The test sled shown is of a narrow gauge rail configuration in which the test sled rides on two parallel rails. The test sled consists of the sled system (including the payload and other structures) and four slippers. The slippers attach the test sled structure to the rails. There are three major rotational directions of motion for the test sled: roll, pitch, and yaw. The three major axes of motion are due to thrust, aerodynamic forces, and structural forces such as vibration and inertial changes due to rail roughness. Thrust accelerates the sled in the forward direction. Aerodynamic and structural forces such as vibration cause vertical and lateral motion of the sled as it is accelerated forward down the track.

A sample rail roughness is shown in Fig. 3. Rail roughness is defined as a change in geometry of the rail from prismatic, flat,

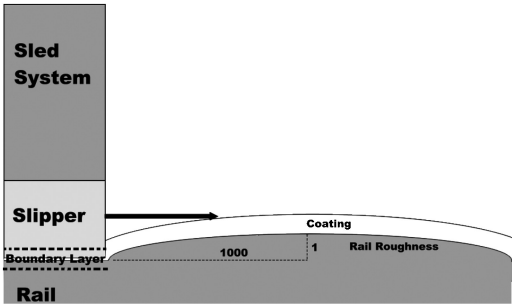

Fig. 3 Schematic of rail roughness, artificial sled system mass, coating, and the boundary layer.

and straight to some eccentricity with a large radius of curvature. The tolerance used at the HHSTT is a 0.05-in. (0.127-cm)-high misalignment of the rail over a 50-in. (127-cm) span. This feature is simulated in this study as a 1 to 1000 ratio of semiminor axis to semimajor axis of a semi-elliptical projection of the rail in the path of the slipper. Figure 3 shows a detail of one slipper with an artificial mass labeled as the sled system. This artificial sled system mass is attached to the slipper to simulate the sled mass that affects the slipper impact on the rail. Figure 3 also shows a coating applied to the rail and rail roughness. Within Fig. 3, one can also see the boundary layer. This is a thin layer of interaction between the slipper and either the coating or the rail, whichever material it is sliding against. Within this thin layer of cells, CTH applies the boundary-layer algorithm that allows deviatoric stresses to form along the interface between the sliding materials. Otherwise, CTH treats the sliding interface between materials as a fluidlike layer with no deviatoric component of stress.

If the test sled structure is not infinitely stiff, the slipper may undergo rotational accelerations and motion in the roll, pitch, and yaw directions. If the slipper undergoes a rotation, a force couple is generated as a reaction to this motion when the slipper rotates through the gap between it and the slipper. The force couple acts opposite in direction to the rotation. The magnitudes of the coupled forces are dependent on the angular acceleration and inertial mass of the test sled that is imparted by the rotational motion. The impulse of the impact will be equivalent to the change in momentum of the slipper and the attached test sled on impact.

Figure 4 shows an example of roll, pitch, and yaw of the slipper and the points of contact in which reaction forces occur. For the roll motion (Fig. 4a), the reaction forces occur at the upper and lower rail corners in which observations have shown that rail gouges usually occur. In addition, these are points of plane strain conditions.

If the slipper rotates upward in a pitch motion (Fig. 4b), the reaction forces would result in point forces at the front bottom of the slipper–rail contact and the top back corners of the slipper–rail interaction. The slipper rotates through the slipper gap between the slipper and the rail until it contacts the corners of the rail. In some cases, depending on the motion of the slipper, these points of contact are the same as what would occur in a roll. This would effectively increase the force at the corners that the slipper and rail undergo.

Figure 4c shows that reaction forces on the slipper due to rotation in the yaw direction occur at the sides of the rail. Here too, observations of actual gouges indicate that gouges most likely occur at these points. The slipper again is limited to rotations through the slipper gap until the slipper strikes the rail at the sides. If the slipper is given a component of yaw in addition to pitch and roll, the slipper could strike on the relatively sharp corner of the rail. These regions are all areas of plane strain because, on impact, the out-of-plane motion of the deformation is restricted. The inertial effects of the impact occur within a two-dimensional plane of action.

Figure 5 shows a real-world example of such an occurrence. The gouge here started on the corner of the rail, which seems to indicate both yaw and either or both roll and pitch motion along with the forward acceleration of the test sled. If this gouged rail is also a portion of the rail that is approximated by a rail roughness, the forces at impact would have been even greater in this area.

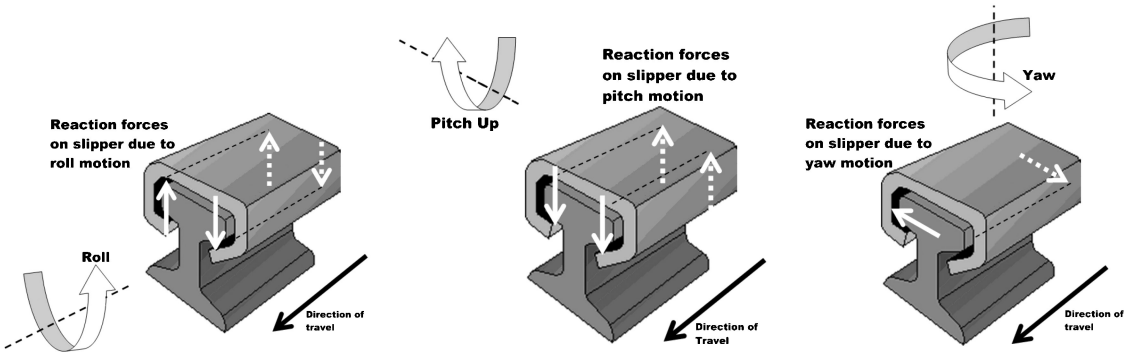

a) Roll motion and reaction forces on slipper **b) Pitch motion and reaction forces on slipper** **c) Yaw motion and reaction forces on slipper**

Fig. 4 Rotations of slipper and reaction forces.

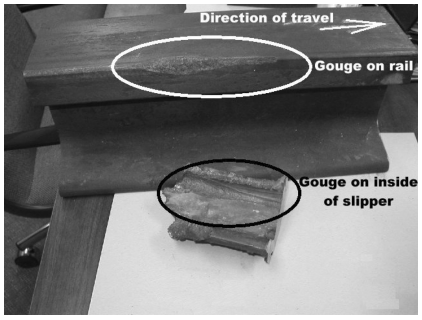

Fig. 5 Actual gouge at reentrant corner of rail in which plane strain condition likely exists at impact.

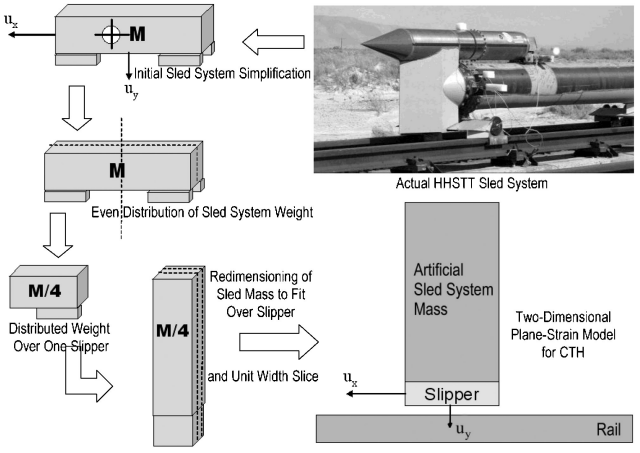

Fig. 6 Simplification of HHSTT rocket sled system into CTH computer model for dimensional and numerical analysis.

With a general character described in the preceding paragraphs, it is now important to represent the appropriate plane strain model. To do this, the three-dimensional HHSTT sled system mass is simplified as a block of bulk material by taking the total mass of the sled system and payload (minus the slippers) and distributing it within a homogeneous block of arbitrary dimensions (Fig. 6). This three-dimensional block is then divided evenly among the four slippers of a sample narrow gauge rail system (neglecting rotations of the sled system), and the body is assumed to translate in the vertical and horizontal directions only. Also, the center of mass is assumed to lie at the geometrical centroid of the artificial sled body.

The three-dimensional artificial sled quarter-mass is then redimensioned with an arbitrary material so that it lies directly over the slipper. The reasoning behind the use of an arbitrary material is that the user may select a material of high density to keep the dimensions of the artificial sled mass to a minimum and provide some relief to computational resources. Shock reflections at the top of the slipper at the interface with the artificial sled system mass will be discussed later. A unit width of this three-dimensional sled–slipper system is then taken as a plane strain two-dimensional sled–slipper system. The resulting model is then translated into a computer model.[7]

The model is transformed onto a two-dimensional vertical plane so that the dynamic analysis and design system (DADS) vertical velocity may be used for the vertical impact velocity. However, actual gouges usually occur on the corners of the rail and not on top of the rail as discussed earlier. Therefore, one must consider whether the model provides for the actual three-dimensional impacts that occur including roll, pitch, and yaw. In any case, whether there is roll, pitch, or yaw, the horizontal velocity will not change. Also, any accelerations are small over the time period being considered so as to be almost zero.

Whatever the direction of impact, the plane strain slice being modeled accounts for a conservative scenario that the plane strain section will see in terms of energy and momentum effects. In essence, a three-dimensional model contains an impact of the sled system mass at some velocity vector along three axes. That impact can be characterized by resultant impact velocities normal to the rail and tangent to the rail within a two-dimensional plane. The mass impacting at the velocity is still the slipper mass coupled with the sled system mass.

In other words, the kinetic energy and momentum the rail and slipper feel at impact are a function of velocity and the sled system mass whether it is due to roll, pitch, or yaw components. These velocities are reduced to a two-dimensional impact within some plane. In both the three-dimensional and the two-dimensional models, the mass of the sled system is the mass that will be impacting the rail with the slipper acting as the transfer mechanism for the impact effects. The conclusions for a two-dimensional plane strain model should also apply to most three-dimensional impacts that are due to roll, pitch, or yaw.

A plane strain model is convenient because it reduces the computational time for a solution. However, one concern is that the plane strain solution may not accurately portray the response of the system because it simulates the impact with infinite thickness. Laird studied the three-dimensional impact of a slipper on a rail with the same out-of-plane dimension, that is, 1 in. or 2.54 cm, as an actual slipper. He found the plane strain assumption to be a conservative approximation of a three-dimensional model.[8] In his study, gouging was found to occur later for the three-dimensional model as compared to the plane strain model. Comparable gouges occurred at 11 μs for the three-dimensional model and 6.5 μs for the plane strain model.

Scaling methods may be used to guide development of the two-dimensional plane strain model into a CTH input model.[9] Furthermore, the invariant products may be used as a set of qualitative guidelines to aid in applying CTH model results to other test sleds. They provide an indication of what parameters of the CTH simulation model need changed to better represent the particular dimensionality of a given test sled.

One difficulty that may arise is a shock reflection off of the interface between the slipper and the artificial sled mass. This would not simulate a condition for the real test sled. Most shocks that reflect off of the top of the slipper will occur due to the density change

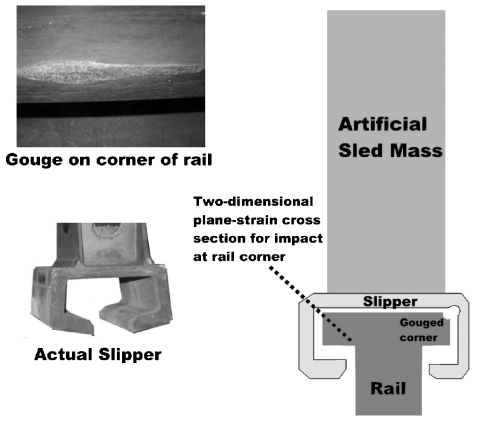

Fig. 7 Slipper plane strain impact corner exposed to low-density medium.

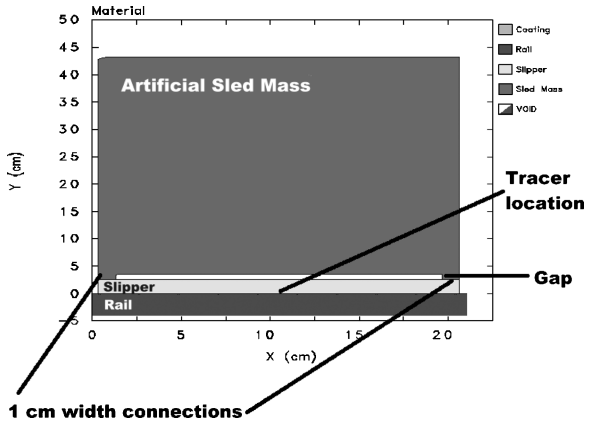

Fig. 8 Gap between slipper and sled mass to simulate shock reflections in real test sled.

for the portion of the slipper exposed to air. How this aspect of the simulation was considered is discussed in the next section.

II. Shock Reflections at Artificial Sled Mass

In a real impact of the slipper against the corner of the rail, the upper surface of the slipper interfaces with air, not with the sled mass. The density of air is much smaller than an artificial sled mass density of platinum, for instance. When a shock front reaches the top of the slipper, the response will be very different if the shock travels into a material of higher density rather than one of a lower density. Before deciding on the CTH models that will be used to conduct the research, the effect of simulating this specific aspect of the real slipper is studied.

Note from Fig. 7, that the slipper that keeps the rocket attached to the rail is exposed to air at the corner that impacts the rail. Impacts at the corners are examples of two-dimensional plane strain conditions that lead to gouging. The requirement for plane strain conditions for hypervelocity gouging to initiate has been explored by Laird[8] in his comparison of two-dimensional and three-dimensional simulations of gouging and earlier in this paper.

Longer runs can cover a time period of 20 μs so that low-pressure shocks have time to travel from the bottom of the slipper to the top of the slipper at the interface with the artificial sled mass. The elastic wave speed of the slipper material is approximately 5 km/s. At this velocity, it will take a stress wave approximately 5 μs to travel from the area of interaction to the top of the slipper where it meets the artificial sled mass. This could affect the solution. Only a small portion of the slipper is covered by the metal strut connecting it to the sled payload (simulated here by the artificial sled mass). Most of the slipper is exposed to air, and the portion covered by metal is in a place where few gouges have been observed to occur.[1]

It is of interest then to explore the effects of a stress wave as it travels within the slipper and strikes the interface with a low-density material. The current model contains a seamless interface between the slipper and the artificial sled mass. A two-dimensional plane strain impact usually occurs on a section of the slipper exposed to air. To model this case, a void is added between the slipper and sled mass. The sled mass remains attached by two end sections (Fig. 8) to the slipper so that momentum and energy of the artificial sled mass will affect the impact of the slipper. The width of these ends is each 1 cm. They are arbitrarily selected dimensions designed to maximize the gapped interface while minimizing concentrations of mass at the ends. Still, this situation causes an uneven distribution of mass over the slipper and results in a concentration of mass over the front and rear portions of the slipper as it impacts the rail.

A short investigation of the effects of the interface between sled mass and slipper was carried out. A mesh convergence study was first carried out.[7] It was found that the smallest mesh cell size that could be obtained for the region of interest is 0.002 cm per side. Any smaller than that and the mesh cell size is approaching the size of dislocation distances of the material, and the applicability of continuum mechanics is in question. Material length scales based on micromechanics have been determined to be around 0.25–20 μm for a variety of metals.[10] This equates to 0.000025–0.002 cm. To avoid this difficulty, the smallest mesh size used to carry out the investigation is 0.002 cm.

The von Mises elastic–plastic and Mie–Grüneisen equations of state models are used to describe the material behavior of the epoxy coating. A tabular equation of state and viscoplastic material constants are not available in CTH for epoxy. The Mie–Grüneisen equation of state approximation is used to describe the volumetric response of the epoxy. In this model, a function [the Grüneisen function, $\Gamma = \rho^{-1}(\partial P/\partial E)_\rho$] is used to describe the relationship between pressure and internal energy at constant density. This results in a linear relationship between pressure and internal energy at constant density. Thus, the pressure is approximated as

$$P(\rho, E) \approx P_R(\rho) + \Gamma(\rho)\rho[E - E_R(\rho)] \tag{1}$$

For the epoxy equation of state in CTH, a predefined material option for epoxy resin is used to select the Hugoniot and Grüneisen material parameters. Ranges for the Mie–Grüneisen equation of state parameters are 1–2.0 cm/g Grüneisen function, 8–9.0 $\times 10^5$ cm^2/s^{2}K specific heat, 1–2.0 g/cm^3 initial density of the Hugoniot, and 2–3.0 $\times 10^5$ cm/s speed of sound.

The von Mises elastic–plastic constitutive model assumes that yielding occurs when the magnitude of the deviatoric stress tensor S is equal to $\sqrt{(2/3)}Y$, where Y is the yield stress of the epoxy material. In this simulation, the model uses a yield stress of 15 MPa for epoxy. The yield surface in principal stress space for von Mises theory is a constant radius cylinder with the hydrostatic line as the longitudinal axis. This can be improved by making the yield stress a function of temperature, strain rate, and strain hardening, but these variations were not included in this investigation.

Table 1 lists the material properties used for the slipper and rail. The Johnson–Cook[11] constitutive model was used to describe the stress–strain relationship for the steel rail and the Steinberg–Guinan–Lund (see Ref. 12) model was used for the maraging steel slipper. These models are an improvement to the von Mises theory described earlier for epoxy.

The Johnson–Cook model is used to determine the yield stress as a function of temperature, equivalent plastic strain, and equivalent plastic strain rate. It is a curve-fitting model:

$$Y = f(T, \varepsilon^p, \dot{\varepsilon}^p) \tag{2}$$

At low and constant strain rates, metals are known to work along the well-known relationship called parabolic hardening[13]:

$$\sigma = Y + \kappa\varepsilon^n \tag{3}$$

The effect of temperature on effective stress can be represented as

$$\sigma = \sigma_r\left\{1 - [(T - T_r)/(T_M - T_r)]^m\right\} \tag{4}$$

Table 1 Material model constants

Johnson–Cook 1080 steel (iron) rail			Steinberg–Guinan–Lund VascoMax 300[a] slipper		
Model constant	Value	Units	Model constant	Value	Units
ρ_o[b]	7.850	g/cm^3	ρ_o	8.129	g/cm^3
A	1.7526×10^9	g/cm · s^2	A	2.06×10^{-12}	g/cm · s^2
B	3.8019×10^9	g/cm · s^2	G_o	7.18×10^{11}	g/cm · s^2
G_o[b]	7.8×10^{11}	g/cm · s^2	Y_o	1.447×10^{10}	g/cm · s^2
Y_o[b]	7×10^9	g/cm · s^2	$Y_{\max}$	2.5×10^{10}	g/cm · s^2
T_M	1835.7	K	T_{mo}	2310	K
C	0.06	——	B	3.15×10^{-4}	1/K
n	0.32	——	n	0.5	——
m	0.55	——	β	2.0	——
			γ_o	1.67	——
			α	1.2	——

[a]Constants not listed are zero. [b]Not used in the Johnson–Cook model, listed for reference.

The effect of strain rate on effective stress can be expressed as

$$\sigma \propto \ell_n \dot{\varepsilon}$$

This model is applicable up to strain rates of 10^5 s^{-1}. Johnson and Cook used these basics to formulate the following relation:

$$Y = \left[A + B(\varepsilon^p)^N\right][1 + C\,\ell_n \dot{\varepsilon}^p]\left[1 - \theta_h^m\right] \tag{5}$$

where

$$\theta_h = (T - T_r)/(T_M - T_r) \tag{6}$$

and where $\ell_n \dot{\varepsilon}^p$ indicates the natural logarithmic function of plastic strain rate $\dot{\varepsilon}^p$. The reference temperature T_r is taken to be room temperature. A, B, C, N, and m are constants that depend on the material.

The Steinberg–Guinan–Lund model is a strain-rate-dependent constitutive model that defines the dynamic yield stress:

$$Y = \left[Y_T(\dot{\varepsilon}^p, T) + Y_A f(\varepsilon^p)\right][G(P, T)/G_o] \tag{7}$$

The work hardening function $f(\varepsilon^p)$ is defined as

$$f(\varepsilon^p) = 1 + \beta\left(\varepsilon^p + \varepsilon_i\right) \tag{8}$$

The thermally activated component of yield is defined in the plastic strain-rate equation

$$\dot{\varepsilon}^p = \left(\frac{1}{C_1}\exp\left[\frac{2U_K}{T}\left(1 - \frac{Y_T}{Y_P}\right)^2\right] + \frac{C_2}{Y_T}\right)^{-1} \tag{9}$$

where C_1 and C_2 are defined in terms of various dislocation mechanics parameters and are specific to the material being modeled.

The shear modulus G is defined as a function of pressure and temperature:

$$G(P, T) = G_o[1 + AP/\eta^{\frac{1}{3}} - B(T - 0.02585\,\text{eV})] \tag{10}$$

where the unit of electron-volts is equivalent to 11,605 K.

Melting is also modeled in the Steinberg–Guinan–Lund constitutive model through use of a modified Lindemann law. The melting temperature T_m is modeled as

$$T_m = T_{mo}\exp[2a(1 - 1/\eta)]\eta^{2(\gamma_o - a - \frac{1}{3})} \tag{11}$$

When the temperature exceeds T_m, melting has occurred, which results in the loss of yield and shear strength. Y and G are then set to minimum values in this case.

A Lagrangian tracer is located in the middle of the slipper and at the interaction between the slipper and rail, yet still within the slipper. Material located at this tracer would most likely be affected by any shock reflections off of the top of the slipper. The comparison of temperature, pressure, and stress deviator plots for the same tracer show that shock reflection/absorption at the interface between the slipper and the artificial sled mass does not have a significant effect on the results over time. The tracer lies within the boundary-layer interaction. The differences become more significant after 6 μs and are minimal in both cases for temperature, which is a result of the increase in energy caused by the additional work in the formation of plastic strain.

The differences are larger in the solutions for pressure. However, this could be due to the concentration of mass effects near the front of the slipper for the case with a gap, which would cause greater magnitude reflections off of the front of the slipper. These reflections would increase strain rate variations in the sliding surface and cause an increase in pressure in the boundary layer due to the rougher surfaces near the middle of the sliding surface. When deviatoric stress is observed, there are larger fluctuations between the solutions for a gapped sled mass and a seamless interface, but this deviation is not very large. The average deviatoric stress over the 20-μs time period between solutions ends up being within 10% of each other.

For the interface with the artificial sled system mass, a higher-pressure compression wave would travel into the higher-density material. However, with a gap at the slipper boundary, the pressure wave reflects back into the slipper as a low-pressure tensile wave and eventually meets up with the compressive interactions at the bottom of the slipper. This would likely cause a release of the higher pressure at this interaction in the slipper. The driving interaction ends up not being the weak shock reflection, but rather the loads generated by deformation of the sliding interaction between the slipper and rail.

The model containing a gap between the slipper and sled mass is a conservative case for rail roughness impacts because of the larger loads at the front of the slipper. This loading is due to the nonuniform distribution of mass over the slipper. To obtain a conservative solution for the case of a rail roughness impact, the gapped model will be used for two subsequent cases.

III. Results and Discussion

The effects of nonequilibrium thermodynamics and coatings for mitigating hypervelocity gouging in the context of the structural dynamic effects discussed earlier are studied in this paper. In support of this objective, two major cases are studied: 1) clean rail roughness impact at 3.0 km/s (with gap as shown in Fig. 8) and 2) coated rail roughness impact at 3.0 km/s (with gap as shown in Fig. 8).

These cases simulate the thermomechanics of an impact on a rail roughness. We are interested in considering techniques for reducing or preventing this detrimental gouging characteristic. One way currently in use at the HHSTT is to coat the railing with epoxy of at least 6-mil (0.01524-cm) thickness. Therefore, the rail will be modeled without a coating, that is, clean, and with a 6-mil coating (which is the minimum thickness in the field) to gain an understanding of the effect of the coating on mitigating gouging. The subsequent paragraphs will discuss the results for these cases.

A shallow vibratory vertical impact of 2 m/s and tangential velocity of 3.0 km/s (called a vibratory impact) on the clean and the coated rail roughness is studied. A vibratory impact is defined as

one impact that might occur due to structural vibrations. A test run might include many such impacts, but only one is being simulated here. It consists of a large tangential component of velocity and a very small normal component. The purpose of this case is to investigate the initiation of gouging for the given test sled. The reasoning behind the tangential velocity of 3.0 km/s is that 3 km/s is the velocity that the HHSTT is striving to reach. The 2-m/s normal impact is obtained from a separate structural dynamics impact based on the entire test sled structure as a mass–spring–damper system and the rail roughness as a forcing function.

The characteristics of the boundary layer on the thermal environment will also be discussed. As the thermal environment develops, and heat is allowed to flow as an irreversible thermodynamic process, it affects formation of plastic deformation through thermal softening in the constitutive model. Shock waves also influence the thermomechanic response of the materials. Large pressure and temperature changes behind the shock can cause phase changes in the materials. The slipper and rail volumetric responses are both defined by a tabular equation of state. This accounts for phase changes of the materials. The epoxy coating equation of state does not account for this possibility, and so the pressure and temperatures will be analyzed manually using the CTH results.

In low-pressure shocks, the distortional response becomes important. The behavior of the system under this stress condition is better characterized by the shear components of the stress tensor. The treatment and influence of these types of shocks on the system are very different from the hydrodynamic treatment and effects of high-pressure shocks.

If a gouge forms, this phenomenon will be analyzed for potential causes. The velocity vectors will be important for this discussion because formation of rotational velocity components in jetting is a strong indication that jetting will initiate. An improved understanding of the formation of gouging will help in the physical understanding of the mitigation of gouging using coatings.

Microanalysis of damaged portions of the rail in the work of Gerstle et al.[2] showed that gouges contain a surface layer of slipper material deposited on top of martensitized rail steel. Subsurface examination of gouges showed that temperatures were high enough to austenitize the steel and that the rail material was severely strained and microcracked. Gerstle et al. believed this to be evidence of catastrophic thermoplastic shear. In thermoplastic shear, the local rate of temperature change causes a strength decrease that overcomes any strength increases from strain hardening. This causes local shear deformations in the material. Local heat generation due to this shearing can be high enough to austenitize steel. If the thin layer of austenite steel is surrounded by a large mass of solid steel, the austenite layer can be quenched rapidly enough to form martensite.

Austenite is formed when steel is heated above 573 K. This phase of the steel is unstable up to approximately 1185 K and transforms in time. If the austenite is cooled extremely quickly, it transforms into martensite. The Gerstle et al.[2] observations provide a couple of observations that can be investigated in this study. First, the temperatures can be checked to determine if they are high enough to form austenite. Another consideration that can be verified through the numerical results is whether, with heat conduction being simulated, the amount of heat generated is greater than the amount of heat conducted away from the deformation.

In terms of the coatings, high-pressure shocks above 20 GPa will cause dissociation of the molecules in epoxy. Because this is not simulated in the equation of state available for use in this model, pressures of the numerical results will be monitored for values that might cause this effect. The glass transition temperature of epoxy is around 400 K. Above this temperature, epoxy transitions into a rubbery state: It softens and becomes viscoelastic. The effect of a rubbery phase on the response of the epoxy is caused by encouraging the formation of shear bands in the epoxy matrix. This has an overall effect of improving the epoxy's toughness. Epoxy also has excellent thermal resistance properties. Therefore, it can absorb heat energy without raising in temperature. A rise in temperature should be followed by a change in state from a glassy to a rubbery phase, which would improve the epoxy's resistance to impact loading.[14]

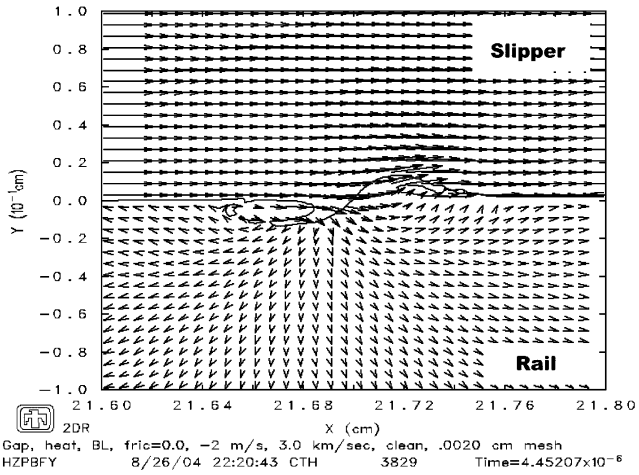

Fig. 9 Velocity vectors at 4.45 μs for point with jetting initiation.

A. Rail Roughness Impact with Clean Rail

In case 1, a short frictional run is made just before impact with the rail roughness. This helps approximate the conditions due to friction just before impact, but does not simulate them exactly. A downward velocity of 2 m/s is chosen to simulate a conservative scenario for the impact. DADS data[15] show the maximum downward velocity for rail misalignments within a 0.001-rad tolerance to be just under 2 m/s. It was found that an impact with a rail roughness at 3 km/s initiated what appears to be a gouge.

According to Laird,[8] jetting is a fluidlike behavior of the slipper material in which "the momentum of the material becomes so high that the slipper material begins to form a material jet that impinges downward into the rail. At this point, this plastic flow also accelerates the growth of the interaction region between the slider [slipper] and rail." This description may be modified to include the rail material that rises up in front of the slipper penetration to penetrate into the slipper material. As the interaction of slipper and rail materials develop further, they form vorticelike rotations. The rotational motion of the material jets remove material from the slipper and rail in the form of a shallow teardrop-shaped gouge as the slipper slides over the rail. In the initiation of jetting, the velocity vectors at the initiation point flow both upward and further forward ahead of the point and both backward and upward behind the point.

In Fig. 9, velocity vectors are shown in terms of magnitude and direction. Smaller vectors indicate smaller magnitudes. The 3-km/s horizontal velocity resulted in jetting formation (with subsequent gouging) at this point. Notice the magnitude of the velocity vectors of the rail material in Fig. 9. The velocities are significantly larger for the rail material when the jet forms. The artificial sled mass and the gap between the mass and the slipper are not shown in Fig. 9 due to the scale. Figure 9 is zoomed in on the portion where jetting occurs.

One indication that the model accurately represents an actual impact is the similarity of martensite formations seen in the Gerstle et al. work.[2] Gerstle et al. observed a 0.03-cm-thick layer of martensite at the trailing edge of an actual gouge. The trailing edge is the point where the gouge begins to form. The gouge had formed from a 173-kg monorail sled test, run at approximately 2 km/s. The sled mass used in this simulation is 202 kg at 3 km/s, with a higher-strength maraging steel slipper. The depth of penetration for temperature changes that provide conditions for the formation of martensite in the simulation is 0.025 cm. This leads to a 0.025-cm-thick layer of martensite during gouge formation. The simulation results show a close approximation of the conditions during actual gouge formation. This assessment is based on martensite formations in an actual gouge under relatively similar test conditions.

Figure 10 shows the temperature contours within the boundary layer near the leading edge of the slipper. The temperatures within the boundary layer in the slipper and rail reach temperatures of nearly 1500 K. The temperatures range in the slipper near the

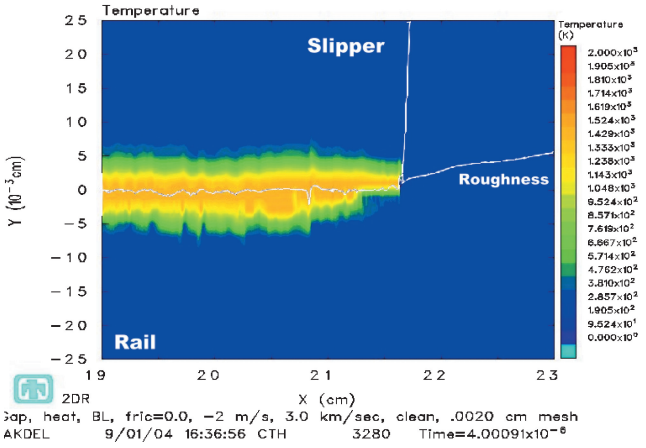

Fig. 10 Temperature at 4 μs just before jetting for 3-km/s case.

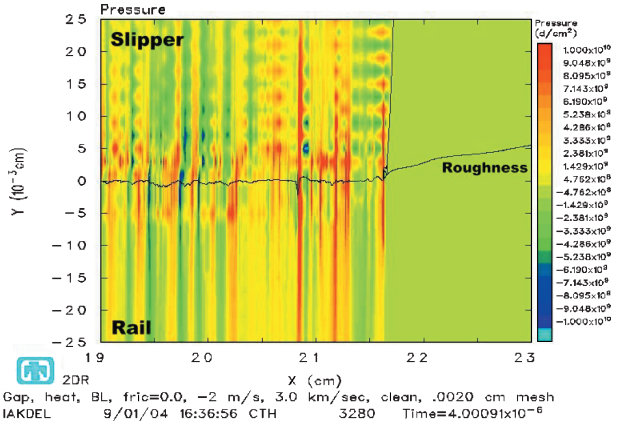

a) Clean rail roughness case

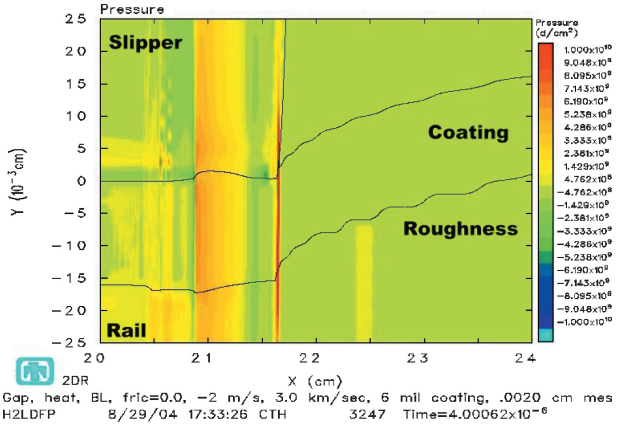

b) Coated rail roughness case

Fig. 11 Comparison of pressures at 4 μs for 3-km/s rail roughness impact.

boundary layer from 500 to 1000 K. The steel is austenitized to both a stable and unstable configuration. On jetting, the temperature rises rapidly from 750 to 1200 K in that region. The increase in temperature lags behind the formation of plasticity in the boundary layer. The response to the rail roughness is dictated by the stresses rather than thermal changes in the material. The rate of heat conduction is much smaller than the rate of plastic formation due to the sliding interaction of the slipper over the rail roughness. Strain hardening effects on the yield strength are at a rate greater than thermal softening effects of temperature changes within the boundary layer.

The potential for fracture within the rail and slipper is also observed, but the values of shear stresses must be greater if this is to occur. By the end of the simulation, the stresses were not high enough to develop plasticity along shear bands. The solution aborted shortly after jetting occurred in the 3-km/s case, and so gouging could not be observed to create cracking or shear band formation in this specific case.

With a better understanding of how gouging initiates and what causes ridgelike deformations between the sliding rail and slipper surfaces, the coated runs can provide insight into how to mitigate gouging. Case 2 is the next case to be discussed. It is the coated case of a vibratory impact on a rail roughness.

B. Rail Roughness Impact with Coated Rail

A basic understanding of the formation of gouging and the effects of coatings in a nonequilibrium thermodynamic environment in which heat is allowed to flow will be applied to the case of a slipper impact on a coated rail roughness. In case 1, jetting formed when the slipper impacted the rail and the geometry of the rail roughness caused the velocity vectors in front and behind the point of origin to rotate upward. This rotation initiated jetting because the plasticized rail and slipper materials impinged further into one another, and the forward velocity of the slipper caused mutual interaction of the two materials. This interaction formed vortices of plasticized slipper and rail material that will result in gouging as the slipper slides further over the rail roughness. In this case, case 2, a coating is added to the rail and acts as a buffer between the slipper and rail. The gap to simulate shock reflections is also present. This shows how coatings react to mitigate the conditions that lead to gouging.

Case 2 has the slipper impacting first the coated rail and then the coated rail roughness at 3-km/s tangential and 2-m/s normal velocities. The 3-km/s clean rail roughness impact resulted in jetting at 4.45 μs. The coated equivalent did not. One consideration is to study what prevented the formation of jetting in the coated case. One obvious possibility is that the coating acted as a buffer simply to prevent the slipper and rail materials from meeting. The following discussion will provide some insight into how this mitigation takes place.

Coating acts to mitigate the magnitude of stress waves and their reflection (as well as their effects on the sliding interface) at impact within the slipper. In the clean rail roughness case, there were varying regions of strain rate within the rail as it reacted to the slipper. The rougher interface dictated these reactions as the slipper slide along. In the coating, by contrast, the strain rate was found to be nearly uniform and the interface smooth. There is a low sloping deformation in the coated case between the slipper and the coating, but the hump was not steep enough to form jetting. Also, parts of the coating ahead of the slipper were ejected forward as the slipper attempted to shear it off. The slipper responded gradually to the deformations in the coating, unlike the discrete and steeper deformations in the clean rail that forced the slipper to react with widely varying strain rates rather than the uniform response seen in the coated case.

The pressure plot (Fig. 11) is one response to these different strain-rate distributions. The pressure fronts in the coated case are more gradual than the clean rail roughness case. With a more gradual response, the conditions in the system are not as extreme in the coated case when compared to the clean case. The pressure front caused by the slipper interacting with the coating does lead to a sharp compressive front in the rail that is otherwise not as large. The transition from a low-density to a higher-density medium results in a strengthening of the shock at impact with the roughness from 2.75 GPa in the coating to about 4 GPa in the rail. This may be a disadvantage of the coating. It helps mitigate the effects of large compressive stress waves that travel from the slipper to the coating, but waves that travel from the coating to the rail increase in pressure. The high-pressure wave that exists in the coated rail is much higher than the wave that is formed in the clean rail (4.5 GPa compared to 1.1 GPa). When this stronger wave travels into the increased area of the rail roughness portion, the pressure drops, but it still remains higher than for the clean rail case. It remains compressive, whereas the wave in the clean case becomes tensile. This

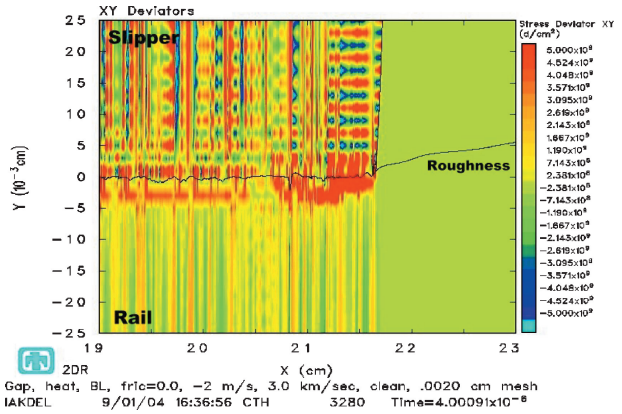

a) Clean rail roughness case

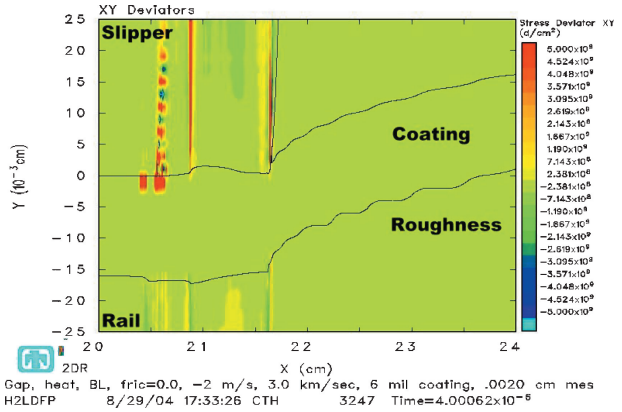

b) Coated rail roughness case

Fig. 12 Comparison of stress deviator at 4 μs for 3-km/s rail roughness impact.

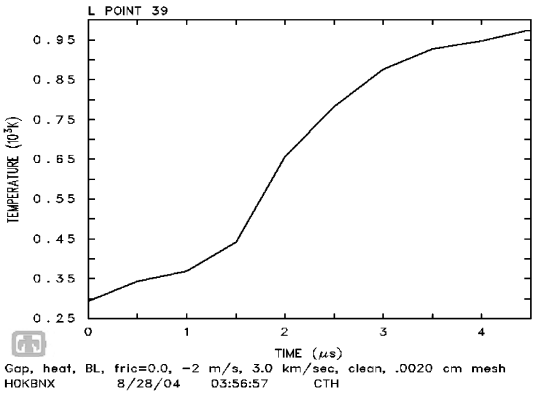

a) Clean rail roughness case

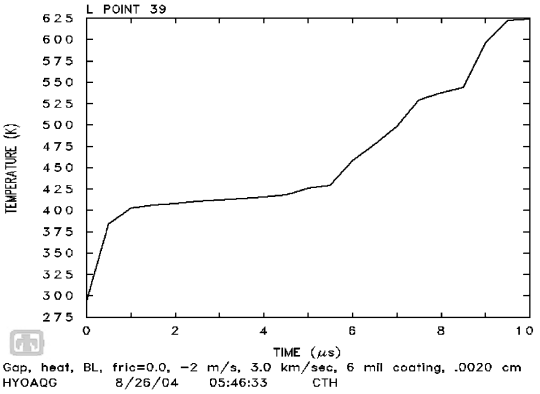

b) Coated rail roughness case

Fig. 13 Comparison of temperature histories in slipper boundary for 3-km/s rail roughness impact.

results in a compressive front that travels into the rail roughness, causing a different set of conditions (higher pressure, temperature, and density) than what exists in the clean rail roughness.

The stress deviator plots (Fig. 12) show an extreme change in the deviatoric stress when a coating is applied to the rail. The deviatoric stresses are nearly all mitigated. This further reduces the conditions leading to jetting because mutual plasticity of the slipper and rail materials is required for jetting to occur. The largest deviatoric stress occurs in a small region of the slipper and appears to be the result of reflections off of the slipper front.

The high temperatures in the slipper boundary layer (Fig. 13) create a thermal gradient that results in heat conduction from the boundary layer to the surrounding material. However, the flow of heat is minimal for the time period studied. Little heat is conducted away from the hot boundary layer, and it continues to increase in temperature as greater plastic work is done in the layer due to the sliding motion of the slipper over the rail and the coating. Because the coating deforms rather than causes the slipper material to deform, the plastic work accomplished in the slipper is less for the coated rail case than for the clean rail case.

The temperature changes in the coating are mainly due to pressure changes within the coating and the formation of plasticity. The temperature at the slipper bottom of the clean rail roughness case reaches a temperature of around 950 K just before gouging (at 4 μs). Conversely, the same point for the coated case only reaches a temperature of 625 K over 10 μs. This temperature is above the flash point of the epoxy, but would only affect the solution if the epoxy could conduct enough heat energy to raise its temperature another 150 K. The coating does reach a maximum temperature near 400 K, which could cause a change of phase to a rubbery state. This phase would be beneficial for reducing the effects of stress, but could raise the effects of frictional heating. This illustrates how the coating works to reduce the temperature effects on the slipper bottom primarily by reducing plastic strain and pressure from impact. If heat conduction was the driver in the development of temperature in the slipper for the rail roughness impact case, the coating would work against the reduction of temperature by insulating the rail and preventing flow from the hot slipper through the coating to the rail.

During slipper impact and sliding over the coated rail roughness, the coating at 3 km/s is ejected in front of the slipper. We also see how the slipper front reacts to the coating. Because more coating material is gathered under the slipper than is ejected in front, a bulged pocket of stored coating material forces the slipper to deform around it. This hump of coating material further acts as a buffer between the rail and the slipper. It helps to allow the slipper to slide over the rail roughness rather than shear the coating away and interact with the steel substrate.

We observe the velocity plot in Fig. 14a to obtain a better understanding of what occurs to prevent gouging. The velocity vectors in the rail are very similar to the vector field seen in the clean (without coating) rail roughness impact cases where the conditions for jetting occur. There are two important differences. In the front portion of the rotation, the direction of the rail material is upward and toward the front of the slipper. Contact with the slipper is prevented by the pocket of coating material that exists under the slipper at that point. As the slipper slides and the rail material continues to move in that direction, more coating material is gathered up to further prevent contact between the slipper and rail. This results in high stresses in the rail in this area (Fig. 14b).

The other difference is the direction of the rail material velocities toward the back of the slipper. Rather than a gradual rotation upward, there is an almost perpendicular change in direction. It appears that the jetting motion of the rail is occurring, but that it occurs inside the rail rather than at the surface of the rail. The coating acts as a buffer preventing mutual interaction of the slipper and rail. The coating is compressed between the slipper and rail and prevents the rail from touching the slipper. The rotational components in this region are not strong enough to break through the coating. The velocity vectors indicate that the coating material is also moving

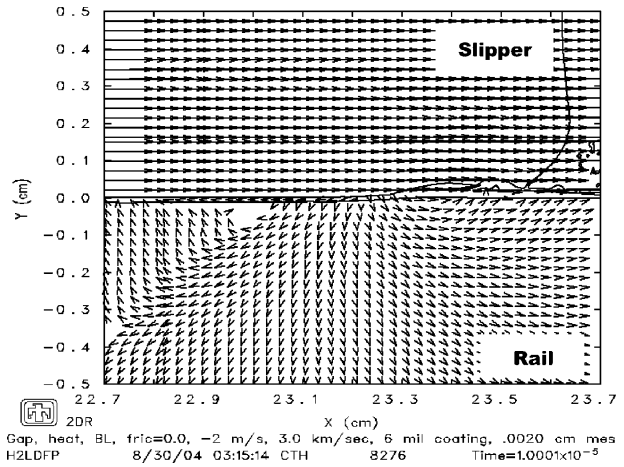

a) Velocity vectors

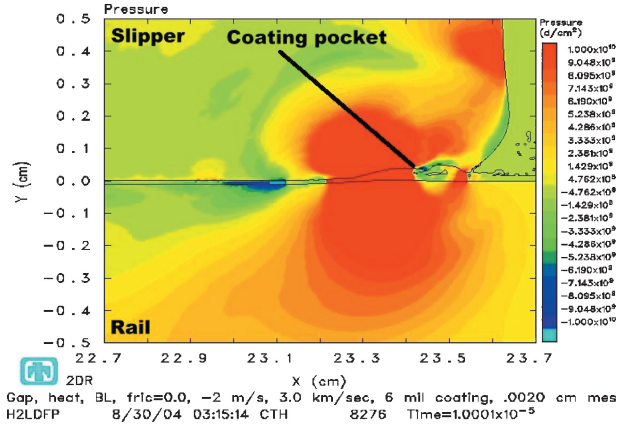

b) Pressure contours

Fig. 14 Comparison of materials and velocity vectors at 10 μs for 3-km/s rail roughness impact; velocity vectors show probable gouging if not for coating effects.

in a direction opposite to that of the slipper. This direction change is small compared to the slipper but is enough to deflect the rail material that attempts to rise into the slipper.

This motion of the coating to the rear appears to be a response to the coating material that is being gathered up and compressed in the front portion of the slipper. As pressure builds up in the coating pocket, coating material is ejected from the front and forced backward to lower-pressure areas. The concept is similar to an air compressor in which a reservoir of compressed air rushes out of a hose to regions of lower pressure. In this case, we have compressed epoxy, which migrates toward regions of low pressure in the $-x$ direction between walls of the slipper and rail material. The velocity of the coating is enough to deflect the rail material and prevent jetting.

This case shows how gouging could initiate through the formation of jetting. It also shows how this can be mitigated by the effects of a coating applied to the surface of the rail. The coating mitigates gouging by reducing the effects of the high-speed impact on the system and by acting as a buffer between the rail and slipper materials. This prevents the rail and slipper materials from jetting. The reason the coating itself does not form this jetting with the slipper is probably twofold. First, the coating material is much softer and deforms rather easily. It deforms rather than causes sharp rigid deformations in the harder materials such as steel. Sharp, rigid projections between the slipper and rail can lead to the conditions that lead to jetting. The other reason the coating does not form jetting is that the thickness is too small to allow the rotational velocity vectors that initiate jetting. The motion of the slipper also forces the coating to react in a fashion that prevents the formation of velocity vectors that are conducive to jetting.

IV. Conclusions

Heating and frictional effects were found to be important to understanding the conditions leading up to jetting (a precursor to gouging). Heat flow was found to be a contributor to cooling in the boundary layer for longer runs. Temperatures were extrapolated for longer contact times from numerical solutions of the shorter time periods. Phase changes due to temperature and pressure were found to affect the slipper and rail due to frictional heating and thermal changes. The steel was found to transform to an austenite phase, as seen in previous observations of actual gouges. The epoxy coating never reached pressures that would cause dissociation of the molecules, but it did reach glass transition temperatures that would cause transition to a rubbery state.

At the temperatures indicated in the CTH solution, steel exists in the austenite phase. Jetting was found to initiate on the impact of the given test sled slipper with a clean rail roughness at 3 km/s. Even before impact, the rail roughness responded elastically to the coming slipper. The slope of the rail roughness decreased slightly a few microseconds before the slipper arrived. The elastic wave speed was faster in steel than the speed of the slipper for the 3-km/s case. This allowed the rail roughness to respond to the slipper before it arrived. The low-pressure compression wave that led the slipper in the rail expanded when it reached the rail roughness, due to the increased area the wave traveled into. The tensile front of this expansion was weak, but it traveled within the rail roughness and affected the region just before the slipper's arrival. This tensile wave was the reason for the rail roughness's change in slope. These waves were then followed by a compressive region that built up to a high-pressure front at the leading edge of the slipper.

It was determined that the gouge formed at 3 km/s because the kinetic energy of the velocity and the high strain rates of the ridges formed at impact provided enough kinetic energy that allowed the velocity vector of the rail to impinge on the slipper and initiate jetting.

A large deformation at the leading edge of the slipper created a pocket of coating material at the leading edge. Rather than shear off coating in a steady stream, the 3-km/s case showed the coating breaking up into pieces as it was ejected in front of the slipper. Also, a greater volume of the coating was gathered and ejected by the slipper at the 3-km/s velocity. This was likely because the 3-km/s slipper was traveling faster than the material sound speed for the coating, and so the coating was unable to respond upstream of the slipper. This resulted in a strong shock wave within the coating and an even stronger shock in the rail. As long as the rail deformation did not penetrate the coating, jetting did not initiate.

The 6-mil epoxy coating was found to mitigate gouging by reducing the stress response to the impact and by acting as a buffer to prevent the rail and slipper materials from interacting with each other. By mitigating ridgelike deformations at the sliding interface, the distortional response within the slipper was less dramatic. Additionally, the coating deformed rather than resisted the sliding slipper material, and so the deviatoric response in the coating was much less than for the clean rail.

The overall effect of the epoxy coating was found to reduce the impact stresses, which reduced the effect of the shock reflections off of the slipper front. This reduction in stress further reduced formation of ridges caused by disparate strain rates along the sliding surfaces. The lower-density coating yielded rather than deformed the slipper. The coating material strained more than the rail material for the same impact velocity vector with the slipper and absorbed more energy, thereby dissipating the impact energy rather than transferring a response to the slipper. The lower-density interface between the slipper and coating also resulted in a tensile pressure wave in the slipper on impact, which further reduced roughness of the sliding slipper surface.

Another effect of the epoxy coating was on temperature. Polymers like epoxy absorb a greater amount of heat before increasing in temperature, as compared to steel. They have increased thermal resistance as compared to steel, but this results in a decreased resistance to impact. The lower temperatures associated with the coated rail meant that the slipper and rail were less likely to transform

into austenite steel. The epoxy absorbed energy without increasing in temperature as much as the steel. The coating reduced the temperature of the slipper sliding boundary in half as compared to the uncoated case. The final temperature of 460 K for this case would not have resulted in the slipper steel entering an unstable austenite phase.

A coating thickness that is at least the height of any estimated rail roughness may be able to mitigate any gouging that is likely to occur at 3 km/s. If a rail misalignment is limited to 0.05 in. (0.127 cm) over a 50-in. (127-cm) length, this could be used as an approximation of the maximum height of any slipper impact with rail material. A coating thickness of at least 50 mil would allow the slipper to slide over any rail roughness without changing the velocity vectors of the rail material, so that it would not impinge on the slipper. The layer of coating that exists between the slipper and rail would also act to prevent the two materials from contacting each other and forming a jet.

To maintain the gap between the slipper and rail of approximately 0.125 in., the thickness of the coating should remain under 125 mil. Otherwise, the coating may plug the gap and cause difficulties with the slipper. It is not known what effect blocking the gap of the slipper and rail will have, but this could cause the development of catastrophic stresses if the front pocket that was seen to form in the slipper increases linearly with the coating thickness.

For example, the height of the pocket of coating that forms at the front edge of the slipper is approximately 0.05 cm for a 6-mil coating that slides over a standard rail roughness after 10 μs. This height is equivalent to approximately 20 mil. If the maximum height of a rail roughness is approximately 50 mil, a linear extrapolation of the pocket height with coating thickness would equate to a desired coating thickness of approximately 15-mil thickness. When it is assumed that the linear extrapolation is correct, this would provide a leading-edge pocket of coating that would allow the slipper to slide over any rail roughness that is within the normal tolerance at the HHSTT for a horizontal slipper velocity of 3 km/s and a vertical velocity of 2 m/s.

When a linear extrapolation is used, the leading-edge slipper pocket of coating material would become as thick as the slipper gap for a coating of approximately 38-mil thickness. Potential difficulties of this occurring include increased stress on the slipper, aerodynamic effects within the slipper gap, and increased stress in the coating that would become magnified as the shock front extends into the steel rail. This magnification of the shock within the coating is a disadvantage of the coating. For the thickness studied, the benefits of the coating outweighed this disadvantage. Therefore, even though increased coating thickness may improve gouging mitigation, there is a limit to the beneficial effects.

A consideration of increasing the coating thickness is that increased thickness would provide more space for the coating material to form rotational velocity vectors that could lead to jetting of the coating into the slipper. If the slipper material is plastic, and enough thermal softening has occurred, then the slipper may flow with the coating, and gouging of the slipper may result. This too requires further study to make definite conclusions about this scenario. Improved coating material models would be extremely helpful in this regard.

Acknowledgments

The authors acknowledge Dean Mook and Neal Glassman from the U.S. Air Force Office of Scientific Research for their generous financial support. The authors also acknowledge the invaluable technical expertise of William Baker of the Air Force Institute of Technology, Robert Brockman from the University of Dayton, and Michael Hooser from the Holloman High Speed Test Track. The views expressed in this paper are those of the authors and do not reflect the official policy or position of the U.S. Air Force, the Department of Defense, or the U.S. Government.

References

[1]Mixon, L. C., "Assessment of Rocket Sled Slipper Wear/Gouging Phenomena," *Slipper Wear and Gouging Phenomena*, by T. Caipen and C. Needham, ARA SBIR Rept. for 846 TS/TGTAD, Applied Research Associates, Inc., Albuquerque, NM, 1997, Chap. 4.

[2]Gerstle, F., Follansbee, P., Pearsall, G., and Shepard, M., "Thermoplastic Shear and Fracture of Steel During High-Velocity Sliding," *Wear*, Vol. 24, April 1973, pp. 97–106.

[3]Graff, K. F., and Dettloff, B. B., "The Gouging Phenomenon Between Metal Surfaces at Very High Speeds," *Wear*, Vol. 14, No. 2, 1969, pp. 87–97.

[4]Hertel, E. S., Bell, R. L., Elrick, M. G., Farnsworth, A. V., Kerley, G. I., McGlaun, J. M., Petney, S. V., Silling, S. A., Taylor, P. A., and Yarrington, L., "CTH: A Software Family for Multidimensional Shock Physics Analysis," *Proceedings of the 19th International Symposium on Shock Waves*, Vol. 3, No. 3, Springer-Verlag, Heidelberg, Germany, 1993, pp. 377–382.

[5]Laird, D., and Palazotto, A., "Gouge Development During Hypervelocity Sliding Impact," *International Journal of Impact Engineering*, Vol. 30, No. 2, 2004, pp. 205–223.

[6]Laird, D., and Palazotto, A., "Effects of Temperature on the Process of Hypervelocity Gouging," *AIAA Journal* Vol. 41, No. 11, 2003, pp. 2251–2260.

[7]Szmerekovsky, A. G., "The Physical Understanding of the Effect of Coatings on the Mitigation of Hypervelocity Gouging AFIT/DS/ENY 04-06," Ph.D. Dissertation, Dept. of Aerospace Engineering, Air Force Inst. of Technology, Wright–Patterson AFB, OH, Oct. 2004.

[8]Laird, D., "The Investigation of Hypervelocity Gouging AFIT/DS/ENY 02-01," Ph.D. Dissertation, Dept. of Aerospace Engineering, Air Force Inst. of Technology, Wright–Patterson AFB, OH, March 2002.

[9]Szmerekovsky, A. G., Palazotto, A. N., and Baker, W. P., "Scaling Numerical Models for Hypervelocity Test Sled Slipper-Rail Impacts," *International Journal of Impact Engineering*, Vol. 32, No. 6, 2006, pp. 928–946.

[10]Voyiadjis, G. Z., Al-Rub, R. K. A., and Palazotto, A. N., "Non-Local Coupling of Viscoplasticity and Anisotropic Viscodamage for Impact Problems Using the Gradient Theory," *Archives of Mechanics*, Vol. 55, No. 1, 2003, pp. 39–89.

[11]Johnson, G, R., and Cook, W. H., "A Constitutive Model and Data for Metals Subjected to Large Strains, High Strain Rates, and High Temperatures," *Proceedings of the 7th International Symposium on Ballistics*, Springer, The Hague, The Netherlands, 1983, pp. 541–547.

[12]Steinberg, D., Cochran, S., and Guinan, M., "A Constitutive Model for Metals Applicable at High-Strain Rate," *Journal of A pplied Physics*, Vol. 51, No. 3, 1980, pp. 1498–1504.

[13]Meyers, M. A., *Dynamic Behavior of Materials*, Wiley, New York, 1994, pp. 325–330.

[14]Pascault, J.-P., Sautereau, H., Verdu, J., and Williams, R., *Thermosetting Polymers*, Marcel Dekker, New York, 2002, Chap. 10.

[15]Hooser, D. M., "Simulation of a 10,000 Foot per Second Ground Vehicle," AIAA Paper 2000-2290, June 2000.

K. Shivakumar
Associate Editor